Eur. Phys. J. Special Topics **224**, 309–318 (2015)

DOI: 10.1140/epjst/e2015-02362-6

THE EUROPEAN PHYSICAL JOURNAL SPECIAL TOPICS

Regular Article

Particle-depletion dynamics in axisymmetric thermocapillary flows

H.C. Kuhlmann[a] and T. Lemée

Vienna University of Technology, Institute of Fluid Mechanics and Heat Transfer, Getreidemarkt 9, 1060 Vienna, Austria

Received 6 August 2014 / Received in final form 16 February 2015
Published online 8 April 2015

Abstract. The removal of suspended particles from the interior of a thermocapillary liquid bridge via a finite-particle-size effect restricting the particle motion near the free surface is analyzed in the framework of a model flow. The particle depletion occurs on the same short time scale as does the particle accumulation in experiments. Furthermore, the time scale diverges in a similar manner for decreasing particle size. The dependence of the time scale for particle accumulation on the particle size is explained in terms of a diverging return time to the free surface for those finite-size particles which are subject to the particle-free surface-interaction.

1 Introduction

The motion of small particles suspended in a fluid is of considerable fundamental and technical interest. In particular, the temporal evolution of the particle concentration field is important for mixing and de-mixing. A very fast and strong de-mixing is observed for micron-sized spherical particles in thermocapillary liquid bridges. The most impressive case is the attraction of the majority of particles to a line-like closed spiral which is rotating about the axis of the liquid bridge with constant rotation rate. This phenomenon has been termed *particle accumulation structure* (PAS) by [1]. It has been shown that such patterns can be caused by particle–boundary interactions [2], inertia effects due to a mismatch between the density of the particles and the fluid [3,4], and by numerical error [5]. Recent investigations of [6] have shown that the experimentally observed time scale for the formation of PAS is consistent with a particle–boundary interaction, in particular acting at the free surface, while the inertia-induced accumulation process is too slow to explain the experimental observations.

Within the particle–free-surface interaction model of [2] it was shown by [7] that the spiralling line-like accumulation pattern is the visualization of only the most impressive attractor out of a class of different attractors. Other attractors are toroidal structures (tubular PAS), period-doubled PAS [8], and strange PAS which denotes the accumulation on a structure which is assumed to be fractal within the particle–free-surface interaction model employed by [7]. A visible property of strange PAS

[a] e-mail: h.kuhlmann@tuwien.ac.at

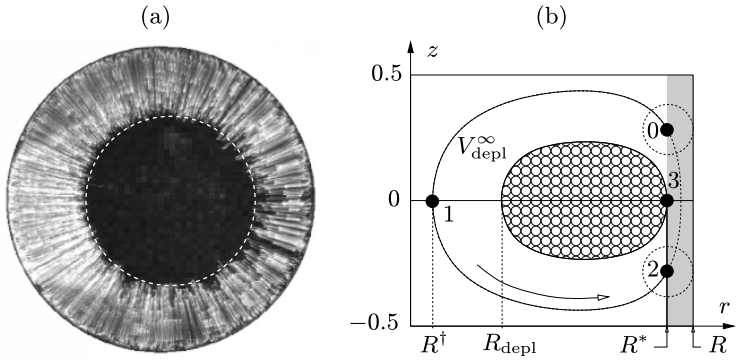

Fig. 1. (a) Experimental visualization (axial view) of the depletion zone in a nominally axisymmetric flow; courtesy I. Ueno and M. Gotoda (Tokyo University of Science). 2-cSt silicone oil, 15-micron diameter gold-coated acrylic particles, particle-to-fluid density ratio 2.0, Pr = 28, Re = 360, $\Gamma = d/R = 0.64$, $R = 2.5\,\mathrm{mm}$, normal gravity, heated from above, volume ratio 1. (b) Sketch of representative streamlines and notation. The flow is anticlockwise (arrow). The grey region is not accessible for particles (dashed circles). The white region becomes depleted for $t \to \infty$ due to particle–free-surface collisions along the cylinder at $r = R^*$ indicated by the bold vertical line. Particles from the textured region are advected without any collision, its border is called release surface. Length scaled by the length of the liquid bridge d.

is the removal of particles from streamlines which approach the free surface closer than a particle radius. As these streamlines also fill the space around the axis of the liquid bridge the accumulation becomes visible by a zone depleted of particles near the axis. In a traveling hydrothermal wave the shape of the projected depletion zone has the same azimuthal periodicity and rotation speed as the underlying flow field. Examples of such depletion patterns can be found in [9]. In fact, the rotating particle-depletion patterns have been employed as indicators signalling a traveling hydrothermal wave [9].

An example for a depletion zone in a nominally axisymmetric flow is shown in Fig. 1a. For subcritical conditions the depletion zone appears in this experiment in less than one second after stirring the particles, and it is axisymmetric. In the course of time the depletion zone becomes slightly offset from the axis in the direction of the incident light as shown in the figure. The broken symmetry is assumed to result from a slightly non-axisymmetric experimental setup.

Since the creation of a particle-depletion zone is the first stage of all PAS and a direct manifestation of the particle–free-surface interaction, we investigate the simplest case and consider finite-size spherical particles density-matched to the liquid and moving in a steady axisymmetric thermocapillary flow in a cylindrical liquid bridge using the collision model of [2]. Of interest are the temporal evolution of the particle accumulation and the properties of the accumulation pattern, in particular the radius of the depletion zone in axial projection.

2 Geometry of the axisymmetric depletion zone

Figure 1b shows a sketch of the geometry and streamlines of the axisymmetric steady flow with velocity field $\boldsymbol{U}$. Within the model of [2] a finite-size particle is perfectly advected by the flow, but the center of a particle cannot approach the free surface closer than a particle radius a. This model is based on the assumption that capillary

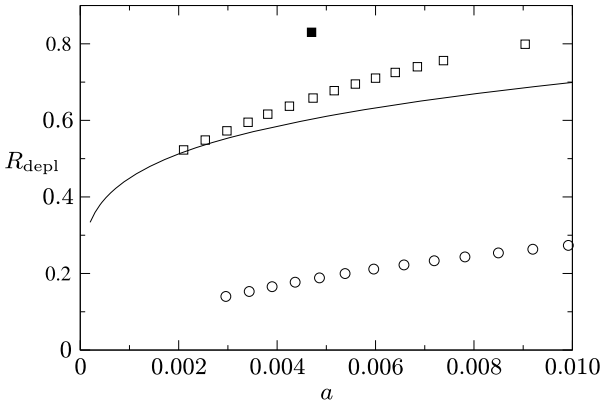

Fig. 2. Radius of the depletion zone in axial projection R_{depl} as a function of the particle radius a (all lengths scaled by the length of the liquid bridge d). Shown are results for the axisymmetric model flow of [7] with Pr = 4, Re = 1800 and $\Gamma = 0.66$ (line, zero gravity) as well as results for Navier–Stokes flows in cylindrical liquid bridges under zero gravity obtained using OpenFOAM for Pr = 8, Re = 800 and $\Gamma = 1.15$ (circles, corresponding to the experiments of [10]) and for Pr = 28, Re = 360 and $\Gamma = 0.64$ (squares, corresponding to the experiment shown in Fig. 1a), both for adiabatic free surface. The solid black square is an experimental result corresponding to the dashed line in Fig. 1a.

and colloidal forces are sufficiently strong to prevent the particle from appreciably deforming the liquid–gas interface. The finite-particle-size effect is only taken into account near the free surface, because the streamlines are extremely crowded there for thermocapillary flows (see also [6]).

We assume that the liquid is initially randomly seeded/marked by particles within the accessible volume which is the volume of the liquid bridge V_0 reduced by the prohibited volume $V_{\mathrm{prohib}} = \{\boldsymbol{x} \mid R^* < r < R, -0.5 < z < 0.5\}$ (grey in Fig. 1b), where $R^* = R - a$ is the radius R of the liquid bridge reduced by the radius a of the particles. As time evolves particles are advected to the cylinder $r = R^*$ (point 2) from where they are transported only by the vertical component of the velocity field. At point 3, characterized by a change of sign of the radial velocity component, they are assumed to be released to the bulk and accumulate on the release surface [7] which is a toroidal stream surface (border of the textured region in Fig. 1b) tangent to the cylinder with radius R^*. The streamline through point 3 which is tangent to the cylinder $r = R^*$ marks the border between the volumes depleted of and occupied by particles, respectively. The minimum radial coordinate of this streamline R_{depl} corresponds to the radius of the depletion zone in axial projection visible in experiments (Fig. 1a).

Assuming model [2] holds R_{depl} provides information about the closest approach to the free surface of this streamline. While the closest approach to the free surface of a streamline (on which advected particles are transported) is very difficult to measure, R_{depl} is very easy to measure. Thus the measurement of R_{depl} together with numerically computed streamlines can be used to predict the maximum radial position of that streamline, and thus to test the validity of the collision model [2].

To estimate the radius of the depletion zone we use the axisymmetric part of the model flow of [7] which has been fitted to the Navier–Stokes flow corresponding to Prandtl number Pr = 4, thermocapillary Reynolds number Re = 1800 and aspect ratio (height-to-radius ratio of the liquid bridge) $\Gamma = d/R = 0.66$ and compare the result with numerical simulations of Navier–Stokes flows. Figure 2 shows the predicted radius of the depletion zone R_{depl} for several flows as a function of the minimum separation from the free surface of the streamline defining the depletion zone, i.e. the particle radius a.

The radius of the depletion zone depends sensitively on the aspect ratio, because the radial extent of the toroidal thermocapillary vortex scales with the height of the zone and not with its radius. Therefore, R_{depl} for a large aspect ratio $\Gamma = 1.15$ is much smaller than for small aspect ratios ($\Gamma = 0.64$). As can be seen the radius of the depletion zone for the model flow [7] ($\Gamma = 0.66$) is very similar to the one obtained by simulation of the Navier–Stokes equations for a comparable aspect ratio ($\Gamma = 0.64$). The experimental value (solid square) determined from the dashed line in Fig. 1a is about 20% larger than the radius predicted by the numerical simulation (open squares). Notwithstanding the experimental and numerical uncertainties, and also the different gravity levels, this result may indicate that the distance between the limiting streamline (release surface) and the free surface is slightly larger than the particle radius. This is consistent with the assumption of [8] that the particle free-surface interaction parameter Δ (minimum distance of the particles from the free surface) is bounded from below by the particle radius a.

3 Particle-depletion process

3.1 Depleted volume

To study the dynamic evolution of the depletion process we consider an incompressible flow with a random particle seeding initially. Since the particle flux density $\eta \boldsymbol{U}$ is proportional to the volume flux density $\boldsymbol{U}$ with particle number density η, we calculate the volume flux through $r = R^*$. The volume (seeded by particles) which has passed through the cylindrical surface $A^* = \{\boldsymbol{x} \mid r = R^*, -0.5 < z < 0\}$ from $t = 0$ to t is given by

$$V(t) = \int_0^t \int_{A^*} H[T(\psi) - t']\ \boldsymbol{U}|_{r=R^*} \cdot \mathrm{d}\boldsymbol{A}\, \mathrm{d}t', \tag{1}$$

where A^* is the cylindrical surface at $r = R^*$ and $\mathrm{d}\boldsymbol{A} = R^* \mathrm{d}\varphi\, \mathrm{d}z$. The heaviside function $H[T(\psi) - t']$ has been introduced, because only the volume marked by particles is of interest. After a turnover time $T(\psi)$, which depends on the streamline defined by the value of the streamfunction ψ, all particles initially located on this streamline between points 0 and 2 (Fig. 1b) will have been removed from the bulk. For $t \to \infty$ the whole volume exterior of the toroidal release surface will have become depleted of particles, i.e. $V(t \to \infty) = V_{\mathrm{depl}}^{\infty}$ (white region in Fig. 1b). In a two-dimensional axisymmetric flow this volume can never be populated by particles again within the model used, because all streamlines within this volume originate from the prohibited region $R^* < r < R$ unaccessible for particles. In a three-dimensional traveling hydrothermal wave a similar but more complicated depleted volume is created bounded by a more complicated release surface [7].

3.2 Turnover time

The turnover time can be easily calculated for the axisymmetric part of the model flow of [7] which has been fitted to the Navier–Stokes flow corresponding to Prandtl number $\mathrm{Pr} = 4$, thermocapillary Reynolds number $\mathrm{Re} = 1800$ and aspect ratio (height-to-radius ratio of the liquid bridge) $\Gamma = d/R = 0.66$. This model has been devised in order to obtain a closed-form and exactly solenoidal approximation of the solution of the Navier–Stokes equations which, in turn, can only be obtained approximately by numerical means and with a certain numerical error, in particular, a divergence error [5]. The mirror symmetry of the axisymmetric model streamlines with respect

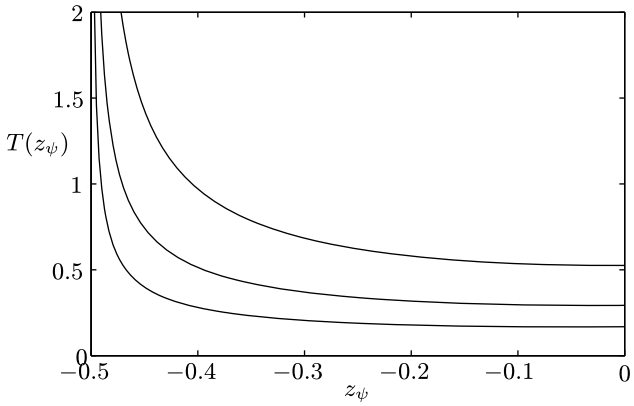

Fig. 3. Turnover times along a closed streamline (except for the fraction in the prohibited region) for $\mathrm{St} = 10^{-4}$, $\mathrm{St} = 10^{-5}$ and $\mathrm{St} = 10^{-6}$ (from lower to upper curve) as function of the vertical coordinate z_ψ of the intersection point of the streamline (collision point) with R^*.

to $z = 0$, as opposed to the slightly broken mirror symmetry of the axisymmetric Navier–Stokes flow, is not expected to have a substantial effect on the turnover time. Similarly, the mean turnover time is not expected to be significantly affected by a slightly supercritical three-dimensional hydrothermal wave, because the wave amplitude is small. As the amplitude of the hydrothermal wave becomes larger, most streamlines will be chaotic [7,8]. Since the hydrothermal wave is periodic in azimuthal direction with only a small amount of nonlinear rectification, it is expected that a suitably defined mean turnover time is little affected by the hydrothermal wave.

The stream function of the steady axisymmetric model flow reads [7]

$$\psi(r,z) = -A_0 r f(r) \cos(\pi z), \tag{2}$$

where lengths, velocities and time are viscously scaled by d, ν/d and d^2/ν, respectively, d being the height of the liquid bridge and ν the kinematic viscosity of the liquid. Moreover, $f(r) = r^n(1-\Gamma r) \geq 0$ for all $r \in [0, 1/\Gamma]$, $A_0 = 11.1$ and $n = 4.74$ as in [7]. The radial and axial velocities are $U(r,z) = -\partial_z\psi/r = -\pi A_0 f(r)\sin(\pi z)$ and $W(r,z) = \partial_r\psi = A_0 g(r)\cos(\pi z)$. The flow is anti-clockwise.

Since the turnover time depends on the streamline, we parameterize the turnover time using the z coordinate $z_\psi = \arccos[-\psi/(A_0 R^* f(R^*))]/\pi$ of the collision point (point 2 in Fig. 1b) of the respective streamline. Due to the mirror symmetry with respect to $z = 0$ of the streamlines the time required for a particle to be advected from point 0 to 2 requires twice the time from point 1 to point 2. With $U = \mathrm{d}r/\mathrm{d}t$, the turnover time becomes

$$T(z_\psi) = 2\int_{t^\dagger}^{t^*} \mathrm{d}t = 2\int_{R^\dagger}^{R^*} \frac{\mathrm{d}r}{U_\psi(r,z)} = \frac{2}{\pi A_0}\int_{R^\dagger}^{R^*} \frac{r\mathrm{d}r}{\sqrt{[rf(r)]^2 - (\psi/A_0)^2}}, \tag{3}$$

where U_ψ denotes the radial velocity on the streamline considered. In the last step we have used (2), i.e. $\sin(\pi z_\psi) = -[1-(\psi/[A_0 r f(r)])^2]^{1/2}$, where the minus sign is due to $z_\psi \leq 0$.

The turnover time as function of $z_\psi < 0$ is shown in Fig. 3 for three particle sizes which are measured using the viscously scaled Stokes number $\mathrm{St} = (2/9)a^2/d^2$. It diverges for $z_\psi \to -1/2$, because the vertical velocity according to (2) approaches

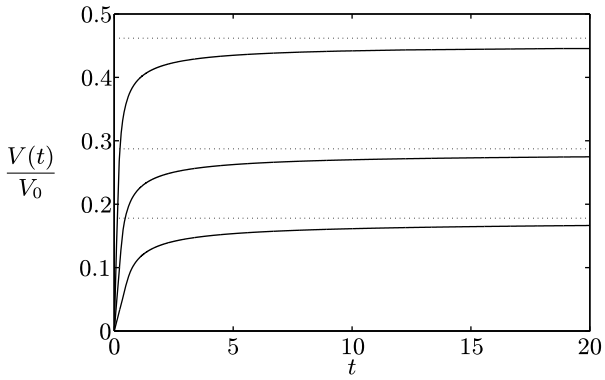

Fig. 4. Volume transported through R^* according to (4) as function of time for Stokes numbers $\mathrm{St} = 10^{-6}$, 10^{-5}, and 10^{-4} (from bottom to top). The volume is normalized by the total volume $V_0 = \pi/\Gamma^2$ of the liquid bridge. The dotted lines represent the time asymptotic values (6) of the depleted volume.

zero on the axis $r = 0$ by construction, while $\boldsymbol{U}$ satisfies free-slip conditions on the walls at $z = \pm 1/2$. A similar and perhaps stronger divergence of the turnover time would result from no-slip boundary conditions on the walls.

3.3 Depletion dynamics

From the model flow (2) and the turnover time (3) the depleted volume (1) is obtained as

$$V(t) = -2\pi^2 A_0 R^* f(R^*) \int_{-1/2}^{0} \tilde{H}(z,t)\, \sin(\pi z)\, \mathrm{d}z, \tag{4}$$

where

$$\tilde{H}[T(z) - t] = \begin{cases} t, & t < T(z), \\ T(z), & t > T(z). \end{cases} \tag{5}$$

The integral in (4) is understood as the principal value. The typical evolution of the depleted volume is shown in Fig. 4 for three different relative particle sizes. For $t \to \infty$ the depleted volume $V(t) \to V_{\mathrm{depl}}^{\infty}$ approaches its maximum. It can be expressed, using the result given in the appendix of [7] as

$$V_{\mathrm{depl}}^{\infty} = V^* - 4 \int_{R^\dagger}^{R^*} \arccos\left(\frac{-\psi^*}{A_0 r f(r)}\right) r \mathrm{d}r, \tag{6}$$

where ψ^* is the value of the streamfunction on the streamline tangent to R^* and $V^* = V_0 - V_{\mathrm{prohib}}$ the volume accessible by particles. To illustrate the depletion patterns particle configurations at $t = 1$ are shown in Fig. 5 for the 2D-model flow (2) and for the full three-dimensional model [7] (for comparison). The particles near the axis move very slowly (the turnover time diverges for $\psi_z \to -0.5$, Fig. 3) and have not escaped from that region at $t = 1$. In an experiment such slowly-moving particles may sediment if not density-matched to the liquid.

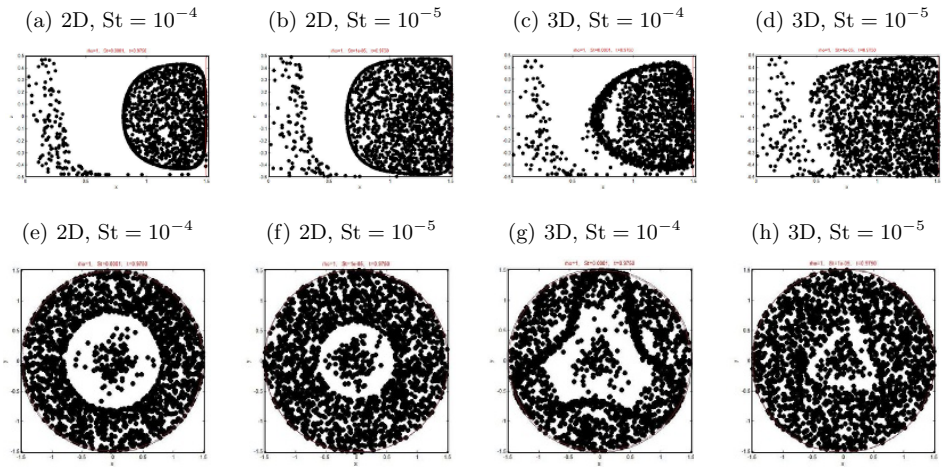

Fig. 5. 2000 particles after $t = 1$ for the model of [7]. Shown are results for the 2D and 3D flows for Stokes numbers $\mathrm{St} = 10^{-5}$ and $\mathrm{St} = 10^{-4}$. Random initial conditions. Particle size not to scale. Top row: azimuthal projection, bottom row: axial projection.

4 Particle-accumulation measures

To measure the evolution of PAS [7] have introduced a the scaled integral deviation

$$K(t) = \frac{1}{2(N - \overline{N})} \sum_{i=1}^{N_{\mathrm{cells}}} \left| k_i(t) - \overline{N} \right|, \tag{7}$$

of the particle concentration from the mean. To determine K the flow is seeded with N particles, the accessible volume is subdivided into N_{cells} equally-sized cells, and the number of particles $k_i(t)$ in the i-th cell at time t is measured. With $N_{\mathrm{cells}} = N$ we have $\overline{N} = N/N_{\mathrm{cells}} = 1$ such that $K_{\mathrm{random}} = 1/\mathrm{e}$ and $K_{\mathrm{max}} = 1$ [7]. K can be evaluated numerically as well as experimentally.

Based on the ratio $V(t)/V^*$ of the depleted volume to the accessible volume initially seeded by particles we calculate K in the limit $N \to \infty$ by noting that the contribution of the depleted volume to the sum in (7) is $\left| k_i(t) - \overline{N} \right| = 1$. The complement of this volume, $[V^* - V(t)]/V^*$ (textured in Fig. 1b), remains occupied for all times by a random arrangement of particles. In the limit $N \to \infty$ the contribution to K is $1/\mathrm{e}$ per cell. Thus we obtain the following expression for K based on the depleted volume

$$K_{\mathrm{depl}}(t) = \frac{1}{2}\frac{V(t)}{V^*} + \frac{1}{\mathrm{e}}\frac{V^* - V(t)}{V^*} + c\frac{V(t)}{V^*}. \tag{8}$$

The first term is due to the depleted volume and the second due to the complement of this volume. The third term takes into account the particles which have been transferred to the toroidal stream surface. It must scale with $V(t)/V^*$, because only those particles occupy this torus which were previously located in the volume depleted at time t. The constant c remains undetermined, because it depends on the surface area of the torus and its coverage with cells. The accumulation signal above the random level is

$$K_{\mathrm{depl}}(t) - \frac{1}{\mathrm{e}} = \left(\frac{1}{2} - \frac{1}{\mathrm{e}} + c \right) \frac{V(t)}{V^*}. \tag{9}$$

Therefore, the signal above the random level based on the depleted volume $V(t)$ should be the same, up to a scale factor, as the value of $K - 1/\mathrm{e}$ obtained by a simulated

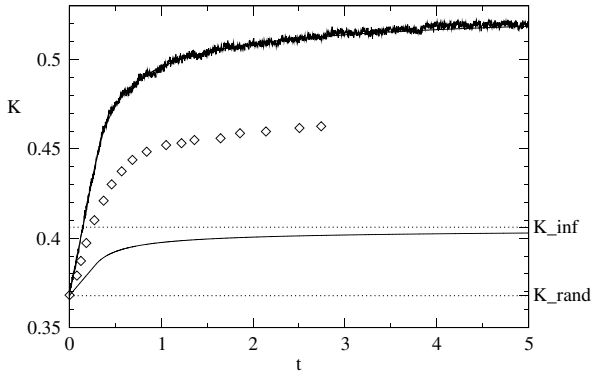

Fig. 6. Accumulation measure $K(t)$ by numerical simulation for St $= 10^{-5}$ using 32000 particles sampled into 200-1-160 bins in radial, azimuthal, and axial directions (noisy curve) and $K(t)$ based on (9) (full curve). The diamonds represent $K(t)$ for the full three-dimensional model of [7], extracted from their Fig. 18a.

motion of particles. This is shown in Fig. 6. The lower full curve shows $K_{\mathrm{depl}}(t)$ for $c = 0$ which can be directly obtained from the depleted volume $V(t)$. In addition its time asymptotic value is indicated (as well as the random level) by a dotted line. The noisy signal represents $K(t)$ obtained from a simulation of 32000 particles initiated at random in the accessible volume V^* and advecting them in the axisymmetric flow (2). The volume has been partitioned into $200 \times 1 \times 160$ cells of equal volumes in radial, azimuthal and axial direction, respectively. Rescaling $K_{\mathrm{depl}} \to 4.3 \times (K_{\mathrm{depl}} - 1/\mathrm{e}) + 1/\mathrm{e}$ yields the upper smooth curve which is identical to the numerical simulation within the noise level. In addition, $K(t)$ for the full 3D model of [7] is shown (diamonds). It is evident that the formation-time scale is practically independent of the presence of the azimuthal part of the flow. Merely, K is smaller in the 3D case, because the release surface has a more complicated structure (see Fig. 28g of [7]).

In order to reduce the information contained in $K(t)$ to a characteristic time of formation of PAS [6] have defined the formation time T_{PAS} as the time at which $K(t)$ has grown to a fraction α of its total variation, i.e.

$$K(T_{\mathrm{PAS}}) = K_{\mathrm{random}} + \alpha\,(K_\infty - K_{\mathrm{random}}). \tag{10}$$

A natural choice for α would be $\alpha = 0.5$. This definition is meaningful if K is a monotonically increasing function, which has been the case for all experiments and simulations of PAS to date. Similarly one can define a depletion time T_{depl} by

$$K(T_{\mathrm{depl}}) = K_{\mathrm{random}} + \alpha\left(K_\infty^{\mathrm{depl}} - K_{\mathrm{random}}\right), \tag{11}$$

where K_∞^{depl} can be evaluated for $c = 0$, because the characteristic time is independent of c. Equation (11) is equivalent to $V(T_{\mathrm{depl}}) = \alpha V_{\mathrm{depl}}^{\infty}$.

As the depletion process primarily depends on the strength of the axisymmetric part of the flow [6] it is tempting to compare the 2D depletion time with the 3D PAS formation time from experiments in order to compare their dependence on the particle size and on the strength of the flow. This comparison is made in Fig. 7 for a typical range particle radii a between the criterion (11) with $\alpha = 0.5$ (circles) and the experimental data of [10] (bold squares and error bars, taken from their Fig. 12) for nearly density-matched particles with density ratio $\rho_p/\rho_f = 1.01$. The data show the same trend but differ in magnitude.

The difference can be explain in terms of the strength of the flow. [6] have shown that the time scale for PAS by way of free-surface collisions is $\propto \mathrm{Re}^{-1}$, because

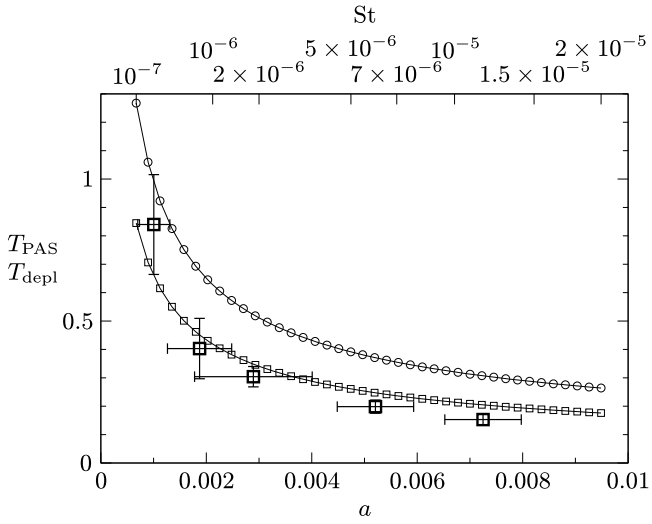

Fig. 7. PAS formation time T_{PAS} and depletion time T_{depl} (both in viscous units) as functions of the non-dimensional particle radius a (in units of the zone height d, lower axis) and corresponding Stokes numbers (upper axis). Shown are theoretical results for T_{depl} for $\mathrm{Re} = 1800$ (circles) and for $\mathrm{Re} = 2800$ (squares) in comparison with the formation time T_{PAS} obtained experimentally by [10] for particle-density ratios $\varrho = 1.01$ (bold squares and error bars), taken from their figure 12 with $\mathrm{Re} \approx 2800$ (see text).

the key quantity determining the time scale is the characteristic (average) frequency (here $\approx 1/\overline{T(z_\psi)}$) at which colliding particles return to the free surface. The same applies to the depletion time. While our analysis was carried out for a thermocapillary Reynolds number $\mathrm{Re} = 1800$, the experimental data of [10] shown in Fig. 7 for a $Na_{0.76}Cs_{0.24}NO_3$ mixed melt are based on $\mathrm{Ma}^{\mathrm{exp}} := \mathrm{Re}^{\mathrm{exp}}\,\mathrm{Pr}/\Gamma^2 = 1.7 \times 10^4$ with $\Gamma = 1.15$. According to [11] the Prandtl number of the mixed melt should not differ much from $\mathrm{Pr} = 8$ of the pure $NaNO_3$ melt. Under this premise the Reynolds number in the experiment can be estimated as $\mathrm{Re}^{\mathrm{exp}} \approx 2800$ which is a factor of $\approx$1.5 larger than Re. However, within our model, the depletion time for $\mathrm{Re} = 2800$ can be obtained just by re-scaling the data for $\mathrm{Re} = 1800$. The result, shown as small squares in Fig. 7, roughly agrees with the experimental data.

5 Discussion and conclusion

Particle accumulation in steady axisymmetric thermocapillary flow in a liquid bridge has been considered in the framework of the particle–free–surface interaction model of [2]. For the model flow of [7] as well as for some Navier–Stokes flows we calculated the radius of the depletion zone in axial view. A comparison of these predictions with experimental data, which are not yet available, would provide a critical test of the particle–free-surface interaction model [2].

Furthermore, the dynamic evolution of the particle-depletion process was investigated for the model flow. The times scales for the creation of the depletion zone based on the depleted volume is the same as the one based on the simulated particle motion. We find a good agreement between the depletion time for axisymmetric flow and the PAS formation time measured by [10] for nearly density-matched particles in a three-dimensional flow if the strength of the flow, i.e. the Reynolds number, is properly taken into account. The strength of the flow is important, because the

characteristic flow velocity is expected to be approximately proportional to the mean eddy-turnover frequency which determines the average particle–free-surface collision rate. The agreement of the depletion time with the PAS formation time is further corroborated by the result for the accumulation measure $K(t)$ computed by [7] from particle simulations for the three-dimensional model flow (Fig. 6).

In qualitative agreement with the experimental PAS formation time we find a strong increase of the depletion time as the particle size gets smaller. As $a \to 0$ the depleted volume shrinks ($R^* \to 1/\Gamma$, $R_{\mathrm{depl}} \to 0$, see Figs. 5a,b,e,f). Since the depleted volume is always bounded by the solid walls and the axis, the average turnover time $\overline{T(z_\psi)}$ of the streamlines in the depleted volume increases strongly (Fig. 3). This leads to the diverging depletion and PAS formation times in the limit. A different divergence of $T_{\mathrm{depl}}(a)$ and $T_{\mathrm{PAS}}(a)$ for $a \to 0$, which is very difficult to pinpoint experimentally, may be caused by the different ways in which the average turnover time diverges: In the model flow with free-slip walls the vanishing axial flow velocity on the axis causes the diverging time scale, while the time scale in the experiments also diverges due to the no-slip condition on the solid walls.

The agreement in magnitude and trend of the depletion time and the PAS-formation time supports the particle–free-surface interaction model of [2], even though further details of a more accurate particle–surface interaction model still need to be developed. The agreement also suggests that PAS becomes visible to the eye in the experiments, because the majority of particles from the volume $V^{\infty}_{\mathrm{depl}}$ are removed within T_{depl} and mapped to streamlines close to the periodic attractor (in case of line-like PAS) [8]. As a result of this particle removal the axial view is cleared on line-like PAS which would otherwise remain partly obscured by the particles moving in $V^{\infty}_{\mathrm{depl}}$.

This work has been supported by the Austrian BMVIT through ASAP9 (project number 840119). We are very grateful to I. Ueno and M. Gotoda (Tokyo University of Science) to allow the reproduction of the image shown in Fig. 1a. H. K. is indebted to D. Schwabe for stimulating discussions.

References

1. D. Schwabe, P. Hintz, S. Frank, Microgravity Sci. Technol. **9**, 163 (1996)
2. E. Hofmann, H.C. Kuhlmann, Phys. Fluids. **23**, 0721106 (2011)
3. D.O. Pushkin, D.E. Melnikov, V.M. Shevtsova, Phys. Rev. Lett. **106**, 234501 (2011)
4. H.C. Kuhlmann, F.H. Muldoon, Phys. Rev. E **85**, 046310 (2012)
5. F.H. Muldoon, H.C. Kuhlmann, Comput. Fluids. **88**, 43 (2013)
6. H.C. Kuhlmann, R.V. Mukin, T. Sano, I. Ueno, Fluid Dyn. Res. **46**, 041421 (2014), ISSN 1873-7005, `http://iopscience.iop.org/1873-7005/46/4/041421`
7. F.H. Muldoon, H.C. Kuhlmann, Physica D **253**, 40 (2013)
8. R. Mukin, H.C. Kuhlmann, Phys. Rev. E **88**, 053016 (2013)
9. I. Ueno, S. Tanaka, H. Kawamura, Phys. Fluids **15**, 408 (2003)
10. D. Schwabe, A.I. Mizev, M. Udhayasankar, S. Tanaka, Phys. Fluids **19**, 072102 (2007)
11. D. Schwabe (2014) (private communication)